Contribution from the Research Laboratories,
Eastman Kodak Company, Rochester, New York 14650

Electronic Calculations of Large Copper Oxide Clusters

R. C. Baetzold

Received June 7, 1988

Large clusters have been embedded in the point charge distribution of the crystal in order to compute the local electronic and ionic structure of copper oxide superconductors. A parameterized CNDO method was employed to consider up to 133 ion clusters. Charge distributions consistent with Cu^{2+} oxidation states were found in models for La_2CuO_4 and $YBa_2Cu_3O_7$ for each geometrically inequivalent site. The valence bands are composed of O 2p components and Cu 3d components with the former at lower binding energy. Oxygen ions are removed most easily from equatorial sites in La_2CuO_4 clusters and from the chain site in $YBa_2Cu_3O_7$ clusters. Substitution of other elements, including F^-, Cl^-, and S^{2-}, for oxygen ions was found most energetically favorable at sites near the chain Cu ion in $YBa_2Cu_3O_7$ clusters.

Introduction

Copper oxide compositions have become of central importance in the high-transition-temperature (T_c) superconductors recently discovered.[1,2] Examples of these oxides include $La_{2-x}Ba_xCuO_4$, $YBa_2Cu_3O_{7-y}$, and $Tl_2Ca_2Ba_2Cu_3O_{10+x}$[3] as representative. Each material contains regular or slightly tilted planes of copper and oxygen ions separated by planes of the other elements. In addition to this characteristic planar Cu-O structure there is a one-dimensional Cu-O chainlike structure in $YBa_2Cu_3O_{7-y}$.[4,5]

The defect properties of the copper oxide materials play an important role in their superconductivity. The $YBa_2Cu_3O_{7-y}$ compound contains varying amounts of oxygen depending upon the conditions of preparation. This oxygen, in the level where y varies from 0 to approximately 0.6, is related to a decrease in superconducting transition temperature.[6] In this compound, sketched in Figure 1, there are five distinct O sites, of which neutron diffraction experiments[4,5] show that four are occupied. In addition there are two distinct sites for Cu ions. One in the copper-oxygen planes contain five oxygen nearest neighbors and is called the Cu_2 site. The other Cu site (Cu_1) in the chain contains four nearest-neighbor O ions, two of which have very short bond lengths. This situation may be compared with the $La_{2-x}Ba_xCuO_4$ system, where the Cu-O local environment consists of a Jahn-Teller axially elongated octahedron characteristic of a d^9 system. It is, therefore, of interest to explore the consequences of these geometric inequalities on the local Cu and O ion electronic properties.

The formal oxidation state picture presents an interesting description of $YBa_2Cu_3O_7$. Using oxidation states of +3 for Y^{3+}, +2 for Ba^{2+}, and -2 for O^{2-} yields an average oxidation state of +2.33 for Cu ions.[7] Some pictures[8] have considered Cu^{2+} in the plane sites (Cu_2) and Cu^{3+} in the chain sites (Cu_1). Other models involve the presence of hole states on oxygen.[9,10] Photoemission experiments have given evidence against the presence of Cu^{3+} oxidation states in the ground state,[9] and some experiments[10] have given support for the hole in hybridized Cu-O states.

Table I. Properties of $Cu_6La_{36}O_{53}^{14+}$ Clusters[a]

A. Electron Populations:	Valence Electrons
Cu	$s^{0.09}p^{0.12}d^{9.51}$
O(a)	$s^{2.0}p^{5.95}$
O(e)	$s^{2.0}p^{5.67}$

B. Energy Required (eV) To Remove O Ion to Infinity	
O(a)	46.9
O(e)	43.5

[a] a and e denote axial and equatorial, respectively.

We will investigate this question as well as the defect properties in clusters representing $YBa_2Cu_3O_7$.

We wish to perform quantum-mechanical cluster calculations that can probe the local ionic and electronic defect structure of $YBa_2Cu_3O_7$ as a means of making comparison to classical atomistic simulation calculations.[11] Several geometrical and physical considerations must be met in the cluster calculations on these materials. First, the Coulomb interactions are long-range and must be explicitly considered in the self-consistent procedure. The long-range nature of these interactions dictates that large clusters be considered in which the boundary ions are terminated in an appropriate field. In addition band-structure calculations[12] have indicated that a significant amount of O 2p and Cu 3d hybridization takes place near the Fermi energy so that effects beyond ionic ones are important. To meet these requirements, we will implement the CNDO method for 100-150-ion clusters that are embedded in the field of the missing ions normally present in the infinite solid.[13]

Method

The parameters employed in this method are shown in the Appendix. We note that O parameters for the valence s and p levels are standard[14] while the Cu parameters for oxidation states such as +2 were not available. To establish these parameters, consider the diagonal elements[15] of the Fock matrix in CNDO for a d orbital on Cu atom A:

$$F_{\mu\mu} = -\frac{1}{2}(I + A)\mu + \frac{\gamma_{dd}}{2}(1 - P_{\mu\mu}) + (10 - Pd)\gamma_{dd} + (1 - Ps)\gamma_{sd} - \sum_{B \neq A} Q_B\gamma_{AB} \quad (1)$$

where $^1/_2(I + A)\mu$ is the average atomic ionization potential and electron affinity, γ_{dd} is the one-center d repulsion integral, $P_{\mu\mu}$ is the occupancy of orbitals μ, Pd is the total d valence population, Ps is the total s and p valence population, Q_B is the charge of adjacent ions, and γ_{AB} is the two-center A,B repulsion integral. We note that the diagonal element may be written

$$F_{\mu\mu} = F_{\mu\mu}^\circ - \sum_{B \neq A} Q_B\gamma_{AB} \quad (2)$$

where $F_{\mu\mu}^\circ$ is exclusively composed of one-center terms. We employ this quantity as a parameter for the various orbitals shown in Table VI.

(1) Bednorz, J. G.; Müller, K. A. *Z. Phys. B.* **1986**, *64*, 189.
(2) Wu, M. K.; Ashburn, J. R.; Torng, C. J.; Hor, P. H.; Meng, R. L.; Gao, L.; Huang, Z. J.; Wang, Y. Q.; Chu, C. W. *Phys. Rev. Lett.* **1987**, *58*, 908.
(3) Sheng, Z. Z.; Hermann, A. M. *Nature* **1988**, *332*, 55.
(4) Beech, F.; Miraglia, S.; Santoro, A.; Roth, R. S. *Phys. Rev. B* **1987**, *35*, 8778.
(5) Beno, M. A.; Soderholm, L.; Capone, D. W., II; Hinks, D. G.; Jorgensen, J. D.; Schuller, I. K.; Segre, C. U.; Zhang, K.; Grace, J. D. *Appl. Phys. Lett.* **1987**, *50*, 1688.
(6) Werder, D. J.; Chen, C. H.; Cava, R. J.; Batlogg, B. *Phys. Rev. B* **1988**, *37*, 2317.
(7) Boyce, J. B.; Bridges, F.; Claeson, T.; Howland, R. S.; Geballe, T. H. *Phys. Rev. B* **1987**, *36*, 5251.
(8) David, W. I. F.; Harrison, W. T. A.; Gunn, J. M. F.; Moze, O.; Soper, A. K.; Day, P.; Jorgensen, J. D.; Hinks, D. G.; Beno, M. A.; Soderholm, L.; Capone, D. W., II; Schuller, I. K.; Serge, C. U.; Zhang, Z.; Grace, J. D. *Nature* **1987**, *327*, 310.
(9) Yarmoff, J. A.; Clarke, D. R.; Drube, W.; Karlsson, U. O.; Taleb-Ibrahimi, A.; Himpsel, F. J. *Phys. Rev. B* **1987**, *36*, 3967.
(10) Horn, S.; Cai, J.; Shaheen, S. A.; Jeon, Y.; Croft, M.; Chang, C. L.; den Boer, M. L. *Phys. Rev. B* **1987**, *36*, 3895.
(11) Baetzold, R. C. *Phys. Rev. B* **1988**, *38*, 11304.
(12) Redinger, J.; Freeman, A. J.; Yu, J.; Massidda, S. *Phys. Lett. A* **1987**, *124*, 469.
(13) Hayns, M. R.; Dissado, L. *Theor. Chim. Acta* **1975**, *37*, 147.
(14) Pople, J. A.; Segal, G. A. *J. Chem. Phys.* **1966**, *44*, 3289.
(15) Baetzold, R. C. *J. Chem. Phys.* **1971**, *55*, 4355.

0020-1669/89/1328-0640$01.50/0

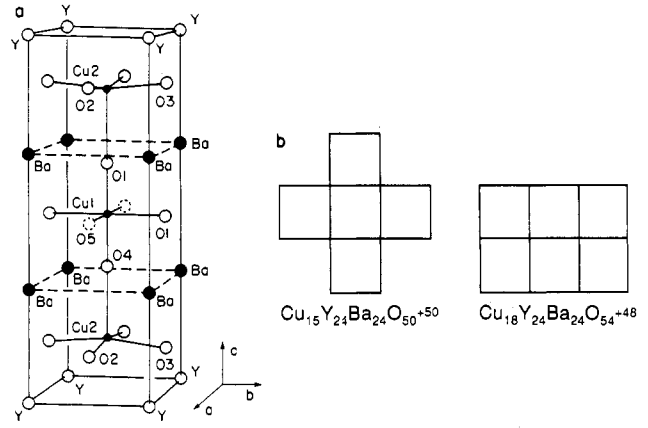

Figure 1. (a) Unit cell of the $YBa_2Cu_3O_7$ compound showing two inequivalent Cu sites and five inequivalent O sites. (b) Arrangements of the unit cells (top view) to form $Cu_{15}Y_{24}Ba_{24}O_{50}^{50+}$ and $Cu_{18}Y_{24}Ba_{24}O_{54}^{48+}$ clusters.

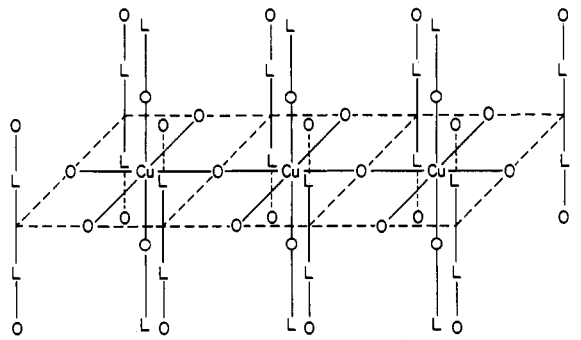

Figure 2. Fragment of the La_2CuO_4 crystal in the form of a $Cu_3La_{22}O_{32}$ cluster. These fragments are aligned adjacently to form the $Cu_6La_{36}O_{53}^{14+}$ and $Cu_9La_{50}O_{74}^{20+}$ clusters studied in this work.

We couple the missing cluster ions to the cluster through the two-center term in eq 2 as has been done in the past.[13] The classical analogue of this term is just the Madelung potential of the missing ions. This calculation is performed with the MOSES code.[16] We will find appropriate parameters for Cu to describe the La_2CuO_4 crystal and then use these parameters for $YBa_2Cu_3O_7$. Closed-shell spin states are studied throughout this paper.

Results and Discussion

A fragment of the La_2CuO_4 structure is shown in Figure 2, from which we construct larger cluster fragments. The central Cu ion has the well-known Jahn–Teller distortion in which axial Cu–O bond lengths are 28% greater than equatorial bond lengths. This leads to a level ordering in the octahedral field in which $d_{x^2-y^2}$ is the highest occupied copper d orbital with half-occupancy. We developed Cu parameters by varying β to achieve the experimental valence bandwidth[17] and $^1/_2(I + A)$ to get appropriate level matching with the O 2p levels. The large clusters $Cu_6La_{36}O_{53}^{14+}$ and $Cu_9La_{50}O_{74}^{20+}$ were employed. A good description of the Jahn–Teller effect is found with the final parameters in the Appendix. Figure 3 shows the energy as the axial Cu–O bond is elongated in $Cu_9La_{50}O_{74}^{20+}$ and $Cu_6La_{36}O_{53}^{14+}$ clusters. An energy minimum occurs at a Cu–O distance that is in close agreement with the experimental distance[18] (2.42 Å).

We now consider the charges and properties of ions within the La_2CuO_4 clusters. Table I shows the electron populations computed for ions within the $Cu_6La_{36}O_{53}^{14+}$ cluster. We observe that the Cu ion has a d orbital Mulliken population of 9.51, which we associate with the +2 oxidation state. The partial occupancy is in $d_{x^2-y^2}$, while the other d orbitals are fully occupied. We do not

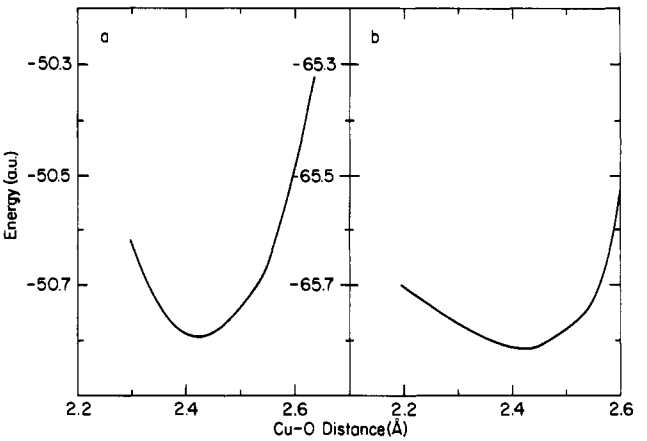

Figure 3. Calculated total energy (au) versus axial Cu–O bond elongation for (a) $Cu_6La_{36}O_{53}^{14+}$ and (b) $Cu_9La_{50}O_{74}^{20+}$ clusters.

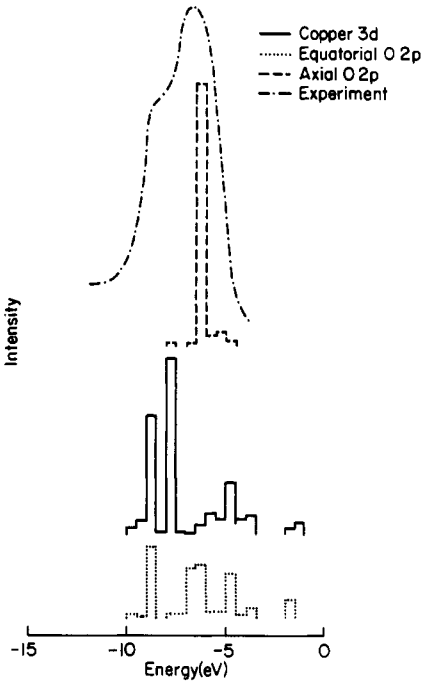

Figure 4. Projection of the density of states for the center Cu atom showing 3d density and axial and equatorial O atoms showing 2p density versus energy. A sketch of an experimental photoemission spectrum[17] is shown for reference.

expect a strict 9.0 population for these d^9 ions because of the procedure for dividing electron density between adjacent ions. In the case of the oxygen ions, the axial oxygen has more negative charge than the equatorial oxygen ions. The energy required to remove an oxygen ion to infinity is less for the equatorial oxygen than for the axial oxygen as shown in Table I. This energy is computed without allowing lattice relaxation, so we only attach significance to the relative values. We note that several other model clusters, including $Cu_9La_{50}O_{74}^{20+}$, which we have considered, consistently give the equatorial oxygen as most easily removed. We note that this result is in accord with experimental results[19] for the parent crystal, where equatorial oxygen vacancies are formed in preference to axial vacancies.

We have considered the components of the valence band density of states for the La_2CuO_4 models. We project from the total density of states the components localized on interior Cu and O ions in order to avoid effects due to surface ions. Figure 4 shows these components for the $Cu_6La_{36}O_{53}^{14+}$ cluster. We observe that

(16) By A. H. Harker, AERE Harwell, Harwell, England.
(17) Shen, Z.; Allen, J. W.; Yeh, J. J.; Kang, J.-S.; Ellis, W.; Spicer, W.; Lindau, I.; Maple, M. B.; Dalichaouch, Y. D.; Torikachvili, M. S.; Sun, J. Z.; Geballe, T. H. *Phys. Rev. B* **1987**, *36*, 8414.
(18) Grande, B.; Muller-Buschbaum, H. K.; Schweizer, M. *Z. Anorg. Allg. Chem.* **1977**, *428*, 120.
(19) For reviews of this see: Williams, J. M.; Beno, M. A.; Carlson, K. D.; Geiser, U.; Ivy Kao, H. C.; Kini, A. M.; Porter, L. C.; Schultz, A. J.; Thorn, R. J.; Wang, H. H. *Acc. Chem. Res.* **1988**, *21*, 1. Holland, G. F.; Stacy, A. M. *Acc. Chem. Res.* **1988**, *21*, 8.

Table II. Madelung Constants[a]

A. La_2CuO_4

La site	7.313	O(a) site	5.217
Cu site	7.551	O(e) site	5.572

B. $YBa_2Cu_3O_7$

	potential 1	potential 2	potential 3
Y site	8.459	7.146	7.308
Ba site	4.598	5.096	5.151
Cu site 1	5.991	6.116	8.263
Cu site 2	7.290	6.408	7.330
O site 1	5.221	4.397	4.944
O site 4	4.929	4.661	5.138
O site 3	5.367	5.946	6.382
O site 2	5.391	5.970	6.422

potential 1: charge on O_1, O_4 = −1.67
potential 2: charge on all O ions = −1.86
potential 3: charge on all Cu ions = +2.33

[a] a and e denote axial and equatorial, respectively.

the deeper states in the valence band are predominately Cu d states while the O 2p components are predominant in the upper part of the band. The axial O 2p components are quite localized compared to the equatorial 2p components, which spread more across the band. A sketch of an experimental ultraviolet photoemission spectrum[17] in the figure shows that the calculated width of the band agrees with experiment.

Figure 1 shows the orthorhombic $YBa_2Cu_3O_7$ experimental unit cell along with arrangements of these unit cells in clusters of $Cu_{15}Y_{24}Ba_{24}O_{50}^{50+}$ and $Cu_{18}Y_{24}Ba_{24}O_{54}^{48+}$ that model this solid. Note that in the smaller cluster an origin unit cell is completely enclosed by its nearest-neighbor cells in the *a,b* plane, unlike the structure of the larger cluster, which is of lower symmetry. Again a potential due to the missing ions is added in classical form to make up for the effect of ions missing from the infinite solid. We employ the Madelung constants listed in Table II for this purpose. These constants are computed from the bulk lattice with the Evjen method using the HADES program.[20] The Madelung constants for La_2CuO_4 and various charge distributions in $YBa_2Cu_3O_7$ are listed in Table II. The neutral basis unit is achieved for one hole distributed on the oxygen ions attached to Cu_1, one hole distributed on all oxygen ions, or the hole distributed on Cu ions, giving an average charge of +2.33. The nominal charges of +3 for Y ions, +2 for Ba ions, −2 for oxygen ions, and +2 for Cu ions are employed elsewhere. We note that the first potential derived from charges of +2 for Cu ions, +3 for Y ions, +2 for Ba ions, −2 for O ions in the plane, and −1.67 for O ions bonded to Cu gives the best fit to the crystal structure in a shell model with short-range two-body potentials.[11] We employ this charge distribution to determine the external potential for the $YBa_2Cu_3O_7$ clusters studied in this work. We comment on other choices of charge distribution in the Appendix.

We consider a $Cu_{15}Y_{24}Ba_{24}O_{50}^{50+}$ cluster formed by symmetrically arranging five unit cells as shown in Figure 1. The computed s, p, d valence populations for Cu and O ions are shown in Table III. We observed that the Cu s, p, d populations are nearly the same on both copper sites and similar to the values observed in La_2CuO_4 clusters. Thus, both copper ions are assigned +2 oxidation states. The average electron charge is slightly larger for O ions at sites O_2 and O_3 in the plane than at O_1 and O_4 sites near the chain Cu. Decomposition of the 3d population shows that the t_{2g} orbitals are almost full on each Cu site. The $d_{x^2-y^2}$ orbital is partially empty at the Cu_2 site with five neighboring oxygen ions, while d_{z^2} predominately contains the partial hole at the Cu_1 site.

We may consider relative energies for removing O^{2-} ions or substituting impurity ions for them. We have not allowed for ionic relaxation around the defect, so relative formation energies are reported in Table IV. We observe that an O^{2-} ion is most easily

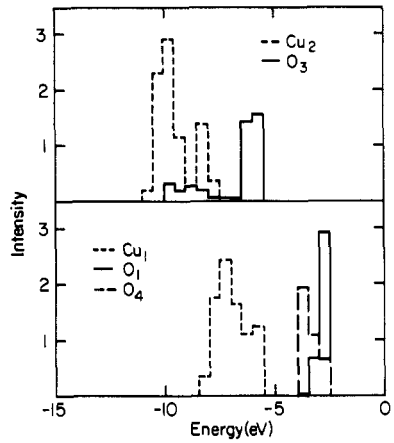

Figure 5. Projection of the density of states for 3d components on the two copper sites and 2p components on three O sites versus energy for $Cu_{18}Y_{24}Ba_{24}O_{54}^{48+}$.

removed from $Cu_{18}Ba_{24}Y_{24}O_{54}^{48+}$ at the O_1 site in the chain as is observed experimentally.[19] When this ion is removed from the chain, the copper ion at site 1 shows an increased electron population characteristic of a d^{10} ion. The substitution of F^- for O^{2-} is energetically most favorable at site 1, while S^{2-} and Cl^- substitution is favored at the O_4 site. These ions appear to substitute preferentially near the Cu_1 ion rather than near the Cu_2 ion in the Cu–O planes.

The projections of the valence density of states on interior Cu and O ions are shown in Figure 5. We observe that the 3d density of state components are similar for the two distinct Cu sites but that the O components are different for each site. The O ions at sites 2 and 3 in the plane are spread more throughout the valence band while the 2p orbitals from O_1 and O_4 are more localized. The copper 3d orbitals on Cu_2 are deeper in the valence band, which correlates with the Madelung constant since the larger Madelung constant is more destabilizing at the Cu_1 site. The Madelung constant is larger for O^{2-} ions in the plane relative to that for chain sites (O_1 or O_4), and this accounts for the greater stabilization for the plane site O^{2-} ions. Note that Madelung potentials are stabilizing for negative charge at an anion site and destabilizing at a cation site, as expected in normal ionic solids. This behavior may be understood from the sign of the leading terms in an expansion of potential at a site within a crystal lattice.

The total bandwidth of the projections of the density of states shown in Figure 5 compares favorably with photoemission experiments. Analysis of band structure calculations[12] and comparison to ultraviolet photoemission experiments have shown the predominant Cu d states more strongly bound than the major O 2p states in $YBa_2Cu_3O_7$.

Cluster calculations[21] for small clusters have been performed with a local spin density method for $Ba_4Cu_2O_7$. A two-peak valence band structure has been found with the more strongly bound peak predominately Cu 3d orbitals and the less strongly bound peak O 2p orbitals. This result agrees qualitatively with our calculations for the $Cu_{18}Y_{24}Ba_{24}O_{54}^{48+}$ cluster in Figure 5. The Mulliken populations for Cu 3d orbitals range from 9.2 to 9.3 in those studies while the numerical integration gives Cu 3d populations of 9.5–9.6. These values also agree well with the values we compute.

Several analyses of the band structure of La_2CuO_4 and $YBa_2Cu_3O_7$ using tight-binding methods have also been presented.[22,23] These calculations have shown the filling of the d-block bands around a given copper ion coordinated to various numbers of oxygen ions. There is substantial agreement of our cluster calculations with these results. One interesting effect[23] concerns the dropping of $d_{x^2-y^2}$ orbitals below the Fermi energy as a chain

(20) Norgett, M. J. Report No. AERE-7650, 1974; Atomic Energy Research Establishment, Harwell, England.

(21) Chen, H.; Callaway, J.; Misra, P. K. *Phys. Rev. B* **1987**, *36*, 8863.
(22) Whangbo, M.-H.; Evain, M.; Beno, M. A.; Williams, J. M. *Inorg. Chem.* **1987**, *26*, 1829.
(23) Burdett, J. K.; Kulkarni, G. V.; Levin, K. *Inorg. Chem.* **1987**, *26*, 3652.

Table III. Valence Electron Population for the $Cu_{15}Y_{24}Ba_{24}O_{50}^{50+}$ Cluster

				3d compn		
	4s	4p	3d	t_{2g}	d_{z^2}	$d_{x^2-y^2}$
Cu site 1	0.199	0.134	9.442	5.991	1.549	1.900
Cu site 2	0.155	0.130	9.539	5.991	1.988	1.560
	2s	2p			2s	2p
O site 1	1.962	5.434		O site 2	1.964	5.512
O site 4	1.967	5.450		O site 3	1.964	5.530

Table IV. Unrelaxed Energies for O Vacancy Formation and Anion Substitution (Relative Values) at Oxygen Sites in $YBa_2Cu_3O_7$

defect	site	rel energy, eV	defect	site	rel energy, eV
O vacancy	1	0.0	F^- substitution	1	0.0
	4	2.76		4	0.77
	2	0.44		2	3.77
	3	3.14		3	2.64
S^{2-} substitution	1	2.98	Cl^- substitution	1	1.19
	4	0.0		4	0.0
	2	5.86		2	8.06
	3	7.23		3	8.23

Table V. Computed Properties of Polaron States in La_2CuO_4 and $YBa_2Cu_3O_7$

	La_2CuO_4			$YBa_2Cu_3O_7$		
polaron	bond[a]	length, Å	d pop.	bond	length, Å	d pop.
Cu^{3+}	Cu^{3+}–O^{2-}(a)	2.134	8.89	Cu_1–O_1	1.746	9.13
	Cu^{3+}–O^{2-}(e)	1.745		Cu_1–O_4	1.715	
Cu^{3+}				Cu_2–O_2	1.796	9.18
				Cu_2–O_3	1.796	
Cu^+	Cu^+–O^{2-}(a)	2.459	9.97	Cu_1–O_1	2.092	9.77
	Cu^+–O^{2-}(e)	2.023		Cu_1–O_4	2.168	
Cu^+				Cu_2–O_2	2.052	9.77
				Cu_2–O_3	2.070	

[a] a and e denote axial and equatorial, respectively.

oxygen ion is removed from site 1. In the present calculations an increase in electron population at Cu_1 filling the d orbitals is observed when this oxygen ion is removed. The two effects seem to agree.

Atomistic calculations[11] have shown that significant lattice ion relaxation takes place in the presence of various charge states of the copper ion. We have examined these small-polaron systems for $YBa_2Cu_3O_7$ and La_2CuO_4 clusters in Table V, where we indicate the computed copper–oxygen bond length. These relaxed ion coordinates are used in CNDO cluster calculations to test the predicted sensitivity of Mulliken charge to lattice distortion. We find a strong coupling. In the case of the Cu^{3+} polaron we compute significant reductions in the d population for copper ions in La_2CuO_4 and at site 1 in $YBa_2Cu_3O_7$. Alternatively, for the Cu^+ polaron the d population is significantly increased over values we assign for the +2 oxidation state. These results show the strong dependence of copper ion charge on lattice distortion in these compounds.

A natural question to ask is whether disproportionation of the Cu^{2+} state can be driven by this lattice coupling. Our calculations[11] for $YBa_2Cu_3O_7$ and earlier work[24] for La_2CuO_4 indicate the reaction is endothermic in both materials when the product ions are separated. However, a type of internally disproportionated complex has shown significant stability relative to that of other bipolaron pairs.[11] This species involves a Cu^+ ion at site 1 and a Cu^{3+} ion at site 2 with the intervening O_4 oxygen ion. The classical calculations, which do not include attractive magnetic interactions,[25] indicate an instability of only 0.22 eV for this type

Table VI. Parameters of the Calculation

atom	config	orbital	exponent	$F_{\mu\mu}°$, eV	$\beta°$, eV
Cu	$d^{9.5}s^1$	4p	1.46	0.67	−1
	$d^{9.5}s^1$	4s	1.46	−0.83	−1
	$d^{9.5}s^1$	3d	1.90	−10.27	−8
O	s^2p^4	2p	2.275	−12.87	−9
	s^2p^4	2s	2.275	−35.85	−9
La	d^0s^0	6s	2.0	−10.21	−1
Ba	s^0	6s	2.0	−6.41	−1
Y	d^0s^0	5s	2.0	−10.21	−1

Table VII. Effect of External Field on the Properties of the $Cu_{18}Y_{24}Ba_{24}O_{54}^{48+}$ Cluster Relative Oxygen Vacancy Formation Energy

	energy, eV			
vacancy	no field	field 1	field 2	field 3
chain O_1	0.00	0.00	0.00	0.00
connecting O_4	1.80	2.26	1.56	0.80
plane O_3	1.74	4.11	3.06	1.65
	Mulliken pop.			
ion	no field	field 1	field 2	field 3
Cu_1	9.46	9.51	9.51	9.41
Cu_2	9.47	9.49	9.50	9.44
O_1	7.38	7.42	7.33	7.55
O_4	7.54	7.52	7.48	7.60
O_2	7.59	7.54	7.54	7.59
O_3	7.65	7.67	7.66	7.69

of disproportionated species, which is similar to that of the disproportionated species described in other contexts.[26] Using the relaxed coordinates from the atomistic calculation, we compute d populations of 9.18 and 9.72 on Cu_1 and Cu_2, respectively, and an instability of 0.12 eV for this complex. We note that the extent of lattice ion distortion strongly influences the stability and charge separation on the copper ions. At smaller distortions where the charge separation is less, the species is stable, while it becomes less stable as the distortion increases. It is possible that such a species would come close to simulating the internally disproportionated complex, where an additional pairing energy due to a loss of spin would be expected.[25]

Conclusions

1. We find that an embedded CNDO calculation of large-cluster models for La_2CuO_4 and $YBa_2Cu_3O_7$ gives +2 oxidation states on each copper ion regardless of geometric and Madelung potential differences among the sites.

2. The copper 3d partial density of states lies more strongly bound than the O 2p partial density of states in each model. The La_2CuO_4 cluster is a typical Jahn–Teller d^9 system with the partial hole in the $d_{x^2-y^2}$ orbital. This is also true at the Cu_2 site in $YBa_2Cu_3O_7$. The Cu_1 site in the latter cluster model contains partial d_{z^2} hole occupancy.

3) Oxygen ions are removed or substituted preferentially in these cluster models. Oxygens at equatorial sites are removed most easily from $Cu_6La_{36}O_{53}^{14+}$, while oxygen is removed most easily from the chain site (O_1) in $Cu_{18}Ba_{24}Y_{24}O_{54}^{48+}$. These results are in accord with experiment. Substitution of S^{2-}, F^-, or Cl^- appears to be preferential near the Cu_1 site rather than the Cu_2 site in the planes.

(24) Islam, M. S.; Leslie, M.; Tomlinson, S. M.; Catlow, C. R. A. *J. Phys. C* **1988**, *21*, L109.
(25) de Jongh, L. J. *Physica C* **1988**, *152*, 171.
(26) Wilson, J. A. *J. Phys. C* **1988**, *21*, 2067.

4. The Mulliken charges of copper ions and lattice ion distortions are strongly coupled. Disproportionation of copper ions is not favored energetically, but an internal complex involving ions representing Cu^+ at site 1 and Cu^{3+} at site 4 is nearly stable.

Appendix

The parameters we have employed are noted in Table VI. Note that the Cu and O ions are treated as suspended in an almost ionic lattice due to the appropriate combinations of Y^{3+}, La^{3+}, or Ba^{2+} ions. Then the additional classical terms due to the charges of ions not present in the cluster are added as Madelung-like terms in eq 2. This classical term does not fully account for termination of the cluster within a periodic field. Earlier work[13] has shown that a significantly reduced value must be chosen to determine effective charges of ions in the external field. A value of 0.23 was employed for LiF. In the case of these copper ion clusters we found that 0.18 was the largest value that would consistently give a converged SCF calculation and we employ this value in all calculations.

We may test whether the charge distribution in the external field is responsible for the effects on cluster charges and oxygen ion vacancy formation energy that we observe. We have thus performed calculations using the Madelung constants for the different external fields from Table II and in the absence of an external field. The results for oxygen vacancy formation and populations are shown in Table VII. In the case of oxygen vacancies the most favorable site for formation is in the chain (O_1). The site in the plane (O_3) is generally least favorable. The Mulliken charges are rather insensitive to the external field. Thus, the intrinsic cluster rather than the external field is dominant in determining these properties. Further calculations of the oxygen vacancy formation energy by the atomistic approach[11] are consistent with O_1 vacancy formation most easily for each of these potential models.

Contribution from the Department of Chemistry and Biochemistry, University of Colorado, Boulder, Colorado 80309

Divalent Rhenium Coordination to Two Radical Schiff-Base Quinone Ligands

Lynn A. deLearie, R. Curtis Haltiwanger, and Cortlandt G. Pierpont*

Received April 12, 1988

Reactions of $Re(CO)_5Br$ and $Re_2(CO)_{10}$ with 3,5-di-*tert*-butylcatechol and ammonia have been investigated. Related reactions carried out with divalent first-row transition-metal ions gave $M^{II}(Cat\text{-}N\text{-}BQ)_2$ compounds, where Cat-N-BQ is a biquinone ligand formed from Schiff-base condensation reactions of 3,5-di-*tert*-butylcatechol and ammonia. In contrast, these reactions produced $Re(CO)_3(C_{28}H_{39}NO_2)(C_{14}H_{21}NO)$, a complex of divalent rhenium with three carbonyl ligands, one anionic monodentate 3,5-di-*tert*-butyl-2-iminophenolate ligand, and one anionic chelating 1-hydroxy-2,4,6,8-tetra-*tert*-butylphenoxazinyl ligand. The complex crystallizes in the triclinic space group $P\bar{1}$ with two complex molecules of slightly different structures per asymmetric unit and unit cell dimensions of a = 12.153 (6) Å, b = 16.376 (14) Å, c = 24.428 (14) Å, α = 107.13 (6)°, β = 102.08 (4)°, γ = 88.85 (6)°, and V = 4539 (5) Å^3. The paramagnetic Re(II) complex exhibits a unique charge distribution, with radical localization on the phenoxazinyl ligand and strong antiferromagnetic coupling between the metal and the radical iminophenolate ligand. The solid-state magnetic moment of 1.31 (2) μ_B is consistent with a spin-orbit-coupled radical, and the isotropic EPR spectrum confirms radical localization on the phenoxazinyl ligand. Mechanistic implications for formation of both radical ligands as well as previously characterized Cat-N-BQ ligands are discussed.

Introduction

Rhenium forms few compounds in the divalent oxidation state, and this is the most poorly characterized of its eight oxidation levels.[1] As with the other lower oxidation states, divalent rhenium shows a tendency to form metal-metal bonds, and much of its chemistry has been focused on the characterization of diamagnetic binuclear phosphine complexes.[2] Mononuclear coordination compounds of rhenium(II) are much less common, again with most containing mono- or bidentate phosphine and arsine ligands.[1b,3] These compounds are paramagnetic with low-spin d^5 configurations, and some, such as *trans*-$ReCl_2(CO)_2(P(n\text{-}Pr)_3)_2$, exhibit EPR spectra characteristic of metal-localized radicals.[3a] In this report we discuss reactions of $Re(CO)_5Br$ with 3,5-di-*tert*-butylcatechol and aqueous ammonia in air, which resulted in formation of a divalent rhenium tricarbonyl complex containing 3,5-di-*tert*-butyl-2-iminophenolate and 1-hydroxy-2,4,6,8-tetra-*tert*-butylphenoxazinylate ligands. Coordination of divalent rhenium to paramagnetic ligands has not been demonstrated previously, and complexation of the iminophenolate and phenoxazinyl radical ligands in the title compound is the first well-characterized example of this coordination.

Scheme I

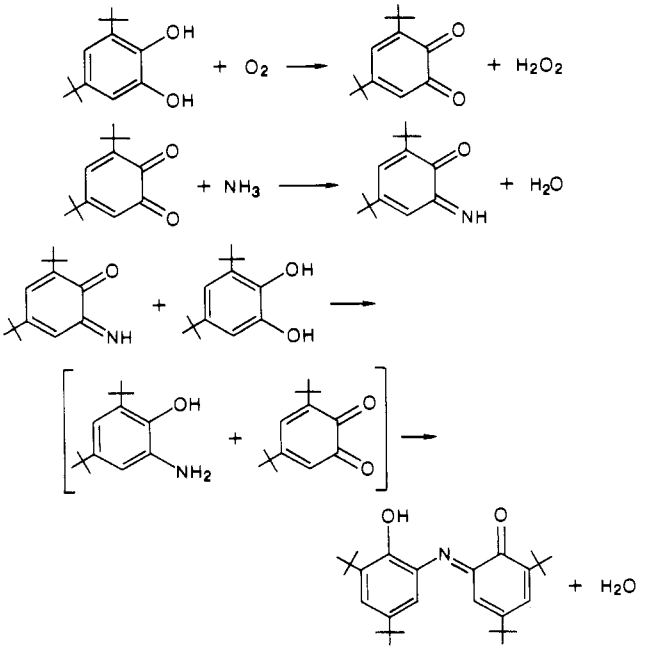

(1) (a) Turp, J. E. *Coord. Chem. Rev.* **1983**, *53*, 249. (b) Fergusson, J. E. *Coord. Chem. Rev.* **1966**, *1*, 459.
(2) (a) Cotton, F. A.; Wilkinson, G. *Advanced Inorganic Chemistry*, 4th ed.; John Wiley and Sons, Inc.: New York, 1980. (b) Heveldt, P. F.; Watson, D. J. *Inorg. Chem. Transition Elem.* **1978**, *6*, 85. (c) Ebner, J. R.; Walton, R. A. *Inorg. Chem.* **1975**, *14*, 1987. (d) Chatt, J.; Rowe, G. A. *J. Inorg. Nucl. Chem.* **1962**, 4019.
(3) (a) Hertzer, C. A.; Myers, R. E.; Brant, P.; Walton, R. A. *Inorg. Chem.* **1978**, *17*, 2383. (b) Chatt, J.; Dilworth, J. R.; Gunz, H. P.; Leigh, G. J. *J. Organomet. Chem.* **1974**, *64*, 245. (c) Chatt, J.; Rowe, G. A. *Chem. Ind.* **1962**, 92. (d) Curtis, N. F.; Fergusson, J. E.; Nyholm, R. S. *Chem. Ind.* **1958**, 625.

0020-1669/89/1328-0644$01.50/0